THE JOURNAL OF BIOLOGICAL CHEMISTRY VOL. 288, NO. 32, pp. 23090–23104, August 9, 2013

Diacylglycerol Kinases Terminate Diacylglycerol Signaling during the Respiratory Burst Leading to Heterogeneous Phagosomal NADPH Oxidase Activation*[S]

Received for publication, January 29, 2013, and in revised form, June 26, 2013 Published, JBC Papers in Press, June 28, 2013, DOI 10.1074/jbc.M113.457606

Daniel Schlam[‡§1], Michal Bohdanowicz[‡§2], Alexandros Chatilialoglu[‡], Benjamin E. Steinberg[‡], Takehiko Ueyama[¶], Guangwei Du[‖], Sergio Grinstein[‡§3], and Gregory D. Fairn[‡‡4]**

*From the [‡]Program in Cell Biology, Hospital for Sick Children, Toronto, Ontario M5G1X8, Canada, the [§]Institute of Medical Science, University of Toronto, Toronto, Ontario M5S1A8, Canada, the [¶]Biosignal Research Center, Kobe University, Rokkodai-cho 1-1, Nada-ku, 657-8501 Kobe, Japan, the [‖]Department of Integrative Biology and Pharmacology, University of Texas Health Science Center at Houston, Houston, Texas 77030, the **Keenan Research Centre of the Li Ka Shing Knowledge Institute, St. Michael's Hospital, Toronto, Ontario M5B1W8, Canada, and the [‡‡]Department of Surgery, University of Toronto, Toronto, Ontario M5S1A8, Canada*

Background: Cell population-based studies obscure potential phagosomal heterogeneity.
Results: We used a dynamic assay to monitor superoxide production in single phagosomes and uncovered variability in NADPH oxidase activity.
Conclusion: The heterogeneity is attributable to variations in local DAG accumulation, which is controlled by DAG kinases.
Significance: Heterogeneity in phagosome responsiveness could enable the survival of a fraction of invading microorganisms.

It is commonly assumed that all phagosomes have identical molecular composition. This assumption has remained largely unchallenged due to a paucity of methods to distinguish individual phagosomes. We devised an assay that extends the utility of nitro blue tetrazolium for detection and quantification of NAPDH oxidase (NOX) activity in individual phagosomes. Implementation of this assay revealed that in murine macrophages there is heterogeneity in the ability of individual phagosomes to generate superoxide, both between and within cells. To elucidate the molecular basis of the variability in NOX activation, we employed genetically encoded fluorescent biosensors to evaluate the uniformity in the distribution of phospholipid mediators of the oxidative response. Despite variability in superoxide generation, the distribution of phosphatidylinositol 3,4,5-trisphosphate, phosphatidylinositol 3-phosphate, and phosphatidic acid was nearly identical in all phagosomes. In contrast, diacylglycerol (DAG) was not generated uniformly across the phagosomal population, varying in a manner that directly mirrored superoxide production. Modulation of DAG levels suggested that NOX activation is precluded when phagosomes fail to reach a critical DAG concentration. In particular, forced expression of diacylglycerol kinase β abrogated DAG accumulation at the phagosome, leading to impaired respiratory burst. Conversely, pharmacological inhibition of DAG kinases or expression of an inactive diacylglycerol kinase β mutant increased the proportion of DAG-positive phagosomes, concomitantly potentiating phagosomal NOX activity. Our data suggest that diacylglycerol kinases limit the extent of NADPH oxidase activation, curtailing the production of potentially harmful reactive oxygen species. The resulting heterogeneity in phagosome responsiveness could enable the survival of a fraction of invading microorganisms.

During phagocytosis, one of the earliest components of the innate immune response, microbial pathogens are engulfed by specialized immune cells into vacuoles known as phagosomes (1). The latter undergo rapid remodeling to acquire an arsenal of microbicidal tools (2). This remodeling, better known as maturation, entails the acquisition of V-ATPases that render the phagosomal lumen acidic, as well as of a variety of antimicrobial peptides, proteases, and lipases that undermine the viability and integrity of the internalized pathogens. Phagosomes also acquire the ability to generate reactive oxygen species. Reactive oxygen species are produced by the phagocyte nicotinamide adenine dinucleotide phosphate (NADPH)-oxidase (NOX),[5] a flavocytochrome-containing complex capable of generating superoxide anions. In turn, superoxide can dismutate into hydrogen peroxide and give rise to hypochlorous acid, all effective microbicidal agents (3).

The oxidase is a multicomponent system composed of two membrane proteins, gp91^{phox} (NOX2; the catalytic subunit)

* This work was supported in part by Cystic Fibrosis Canada, Canadian Institutes for Health Research Grants MOP7075 and MOP93634, and St. Michael's Hospital New Investigator Fund (to G. D. F.).
[S] This article contains supplemental Videos 1–5.
[1] Supported by a studentship from Cystic Fibrosis Canada.
[2] Supported by an M.D./Ph.D. scholarship from the Canadian Institutes of Health Research.
[3] Current holder of the Pitblado Chair in Cell Biology at The Hospital for Sick Children.
[4] To whom correspondence should be addressed: Li Ka Shing Knowledge Institute, St. Michael's Hospital, 209 Victoria St, Toronto, Ontario M5B1W8, Canada. Tel.: 416-864-6060 (Ext. 77330); Fax: 416-864-5167; E-mail: fairng@smh.ca.

[5] The abbreviations used are: NOX, NAPDH oxidase; DAG, diacylglycerol; DGK, diacylglycerol kinase; DGKi, diacylglycerol kinase inhibitor; PA, phosphatidic acid; PtdIns(3)P, phosphatidylinositol 3-phosphate; PtdIns(3,4,5)P_3, phosphatidylinositol 3,4,5-trisphosphate; PLD, phospholipase D; NBT, nitro blue tetrazolium; DIC, differential interference contrast.

and p22^{phox}, three cytosolic regulators, p40^{phox}, p47^{phox}, and p67^{phox}, and a Rho GTPase (either Rac1 or Rac2). During phagocytosis, critical inflammatory signals trigger recruitment of the cytosolic components to the plasmalemma, where they interact with the flavocytochrome, thereby inducing formation of an active NOX complex (4).

Several membrane lipids have been implicated in the regulation of NOX activity, including diacylglycerol (DAG) and phosphatidic acid (PA) (5). DAG can be generated through hydrolysis of phosphoinositides by phospholipase C or by the combined actions of phospholipase D (PLD) and PA phosphohydrolases. DAG promotes recruitment of PKC to the phagosomal membrane and its subsequent activation, which allows for phosphorylation of p47^{phox} (6, 7) and assembly of the active oxidative complex. PA, which can be produced by the hydrolytic action of PLD on phosphatidylcholine and through phosphorylation of DAG by diacylglycerol kinases (DGKs), has also been implicated as a second messenger in the activation of the respiratory burst oxidase (8).

Although much progress has been made in the characterization of the molecular signals upstream of NOX activation, the vast majority of these studies have relied on population-based assays. Such analyses obscure potential heterogeneity in the oxidative response and inherently assume that all phagosomes respond similarly to pathogenic invaders. However, compelling novel evidence suggests that each phagosome is a discrete, independent compartment whose fate is dictated by the unique set of signaling cues that originate at its membrane (9). The observation of heterogeneity in the phagosomal pool prompted us to investigate NOX activity in individual phagosomes. To this end, we devised a dynamic assay to quantitatively monitor oxidase activity in single phagosomes of live cells during the course of particle ingestion. These measurements revealed a striking variability between phagosomes in different cells and even within the same cell. We proceeded to analyze the source of the heterogeneity, placing particular emphasis on the lipid mediators of oxidase activation. Our data indicate that variations in the local accumulation of phagosomal DAG are the main source of the variable oxidative response and that phosphorylation by DGK is a critical determinant of DAG concentration at the phagocytic cup. These observations have important implications regarding the fate of pathogens that are confronted by professional phagocytes.

EXPERIMENTAL PROCEDURES

Reagents—Zymosan A particles (from *Saccharomyces cerevisiae*), human serum IgG, nitro blue tetrazolium (NBT), and lipopolysaccharide (LPS from *Salmonella enterica* 595) were purchased from Sigma. 16% paraformaldehyde (used in PBS at 4% v/v) was from Electron Microscopy Sciences (Hatfield, PA). Alexa Fluor 555-succinimidyl ester was from Invitrogen. Cy5-conjugated and DyLight 488-conjugated donkey anti-human secondary antibody and donkey serum were from Jackson ImmunoResearch. Compounds R59 022 (DGKi I, 30 μM) and R59 949 (DGKi II, 30 μM) were purchased from Enzo Life Sciences, Inc. Dioctanoyl ethylene glycol (100 μM) was from Tocris (Ellisville, MO). Ionomycin (1 μM) was from Calbiochem. PA (L-α-phosphatidic acid; 840074) was purchased from Avanti (Alabaster, AL) and dried under nitrogen gas before being resuspended in serum-free DMEM complemented with 4 mg of essentially fatty acid-free BSA (Sigma).

Cell Culture and Transfection—RAW 264.7 macrophages and HeLa cells were obtained from the American Type Culture Collection (ATCC) and grown in DMEM supplemented with 10% heat-inactivated fetal bovine serum (Wisent, St. Bruno, Canada) at 37 °C in a 5% CO_2-regulated incubator. Cells plated on glass coverslips were transiently transfected using FuGENE HD (Roche Applied Science) according to the manufacturer's protocol. Each well of a 12-well plate was treated with 1 μg of plasmid cDNA and 3 μl of FuGENE HD. Transfected cells were typically used 18–24 h after transfection. Where indicated, macrophages were activated by overnight treatment with 100 ng/ml LPS. For live imaging, cells were incubated in HEPES-buffered RMPI at 37 °C.

Constructs—The DAG biosensor consisted of an N-terminal GFP fused to the C1 domain of PKCδ in the pEGFP(C1) vector. Where indicated, an mCherry fluorophore was used to replace GFP in this vector. The PA biosensor consisted of GFP fused to two PA-binding domains of the yeast protein Spo20p, described previously (10, 11), arranged in tandem, and modified by including the N-terminal nuclear export signal of PKI-α. Plasmids encoding HA-tagged PLD1, wild-type PLD2, and dominant-negative PLD2(K758R) were provided by Dr. J. Brumell (Hospital for Sick Children, Toronto, Ontario, Canada). The surface charge probe, RFP-R-pre, as well as the PtdIns(3)P and PtdIns(3,4,5)P_3 probes were described earlier (12, 13). DGK-GFP isoforms α, β, γ, δ, ϵ, and ζ have also been reported previously (14). DGKθ, originally encoded in the pCMV-SPORT6 vector and provided by RIKEN BRC through the National Bio-Resource Project of MEXT, Japan (15), was digested with EcoRI and XhoI and directionally subcloned into the EcoRI and SalI sites of pEGFP(C3).

Site-directed Mutagenesis of DGKβ—An inactive (kinase-dead) form of diacylglycerol kinase β was generated by primer-directed mutagenesis of the enzyme's ATP-binding site using the QuikChange site-directed mutagenesis kit (Stratagene), conforming to the manufacturer's instructions. Briefly, forward and reverse mutagenic primers (each carrying two complementary point mutations) were utilized to introduce a glycine to aspartic acid transition at residue 495. 10 ng of template DNA (wild-type DGKβ carried in the vector pEGFP(C1)) were used for PCR-based amplification (16 cycles total) of the mutant construct. PCRs were subsequently incubated with the restriction enzyme DpnI to digest the parental wild-type vector while maintaining the integrity of unmethylated linear amplicons. Finally, mutant vectors were transformed into XL1-Blue supercompetent cells for nick repair and plasmid replication. The following were used: DGKβ(G495D) forward, 5′-tagcatgcggtggagatgatactgtgggctggattttg-3′, and DGKβ(G495D) reverse, 5′-caaaatccagcccacagtatcatctccaccgcatgcta-3′.

RT-PCR—One-step RT-PCR was employed to detect transcription of distinct murine DGK isoforms (α through κ) using RNA purified from RAW 264.7 macrophages as template for the cDNA generation. For each reaction, RNA was isolated from 8×10^5 cells using the Qiagen RNeasy mini kit, as instructed by the manufacturer. The Invitrogen OneStep RT-

TABLE 1

Primer sequences utilized for reverse transcription and amplification of DGK isoform-specific mRNA in RAW 264.7 macrophages

The abbreviations used are as follows: Fwd, forward; Rev, reverse.

DGK isoform	Primer sequence	Expected amplicon length
		bp
α	Fwd, 5′-AAGGAAGCGTTGACAGCTGGAAGC Rev, 5′-TTCTGGCCGGCCACCTTCTAGG	502
β	Fwd, 5′-CATCACCTACACCATGACAAACCAGG Rev, 5′-CATTCGAGGTACTCTGCCACGTGC	558
γ	Fwd, 5′-GCGCAACCAAGTGTTGCATGGT Rev, 5′-AGACATTGGGCTCACTACTGCTGGC	507
δ	Fwd, 5′-CAAGAGGAGGTACTTTAAGCTTCGAGGG Rev, 5′-AATAGGTTGGCCGTGCATGGG	320
ϵ	Fwd, 5′-TTCTGCAGGCAGCAGTGTGGC Rev, 5′-CATTACCTGTTCCCAGAGGTAAGACCG	526
ζ	Fwd, 5′-GACCAAGCGGCGCTTCCC Rev, 5′-CAGCTGATGGCTACGATCTCCTTGC	514
η	Fwd, GCAAACCAGCTCTTTCCAAAGGTGG Rev, GCAGTTGTTTGTTGCCCTCACTGC	454
θ	Fwd, AGTGCCTGAAGCAGGTGAAGACCC Rev, AGGCAGTACCATGGAGCGTAGACG	440
ι	Fwd, GAGAATGCTGTGAATGGGGAGCAC Rev, CCTTAATGATCCAGGTGGGCGG	469
κ	Fwd, ACAATTGATCTGTCTCAAGTTGTTTTGGC Rev, CCCTAGGGTCGCTCAGTGCCG	458

PCR kit was utilized for cDNA generation and subsequent PCR amplification; reverse transcription of DGK transcripts was performed with 1 μg of purified RNA template per reaction, using isoform-specific primers for 30 min at 55 °C. The primary sequences of forward and reverse primers utilized in this study are listed in Table 1. Reverse transcriptase was inactivated, and Taq polymerase was activated by increasing the reaction temperature to 94 °C for 4 min. PCR amplification was performed for 40 cycles at denaturing, annealing, and extension temperatures of 94, 55, and 68 °C, respectively.

Phagocytosis—RAW 264.7 macrophages were grown on glass coverslips placed in 12-well plates with DMEM supplemented with 10% heat-inactivated fetal bovine serum. Before the experiments, the coverslips were transferred to Leiden chambers and bathed with HEPES-buffered medium RPMI 1640. The chamber was subsequently placed in a holder mounted on the microscope stage. To initiate phagocytosis, 80 μl of zymosan particles (original concentration = 2 mg/ml) that had been freshly opsonized with human IgG and/or labeled with Alexa 555-succinimidyl ester ([final] = 3 μg/ml) were added to the cells. Where indicated, phagocytes were incubated with nitro blue tetrazolium ([final] = 1 mg/ml). For opsonization, zymosan particles at a concentration of 2 mg/ml were incubated for 60 min with human IgG ([final] = 5 μg/ml). When synchronization of phagocytosis was sought, glass coverslips remained in 12-well plates, and opsonized zymosan particles were added and rapidly sedimented onto the cells by centrifugation at 1,000 rpm for 1 min in a tabletop centrifuge. Excess particles were removed by washing three times with PBS. When required, zymosan particles that remained adhering externally to the macrophages were identified by immunostaining with Cy5-conjugated anti-human IgG at 4 °C for 5 min. Donkey serum was diluted to 10% in PBS and used for 10 min for blocking prior to staining of noninternalized IgG-opsonized phagocytic targets. Where indicated, cells were treated with diacylglycerol kinase inhibitors for 20 min before initiation of phagocytosis.

Fluorescence-activated Cell Sorting (FACS)—In preparation for FACS analysis, zymosan particles were either opsonized with human IgG or labeled with Alexa Fluor 555-succinimidyl ester using the opsonin and labeling dye concentrations described above for phagocytosis assays. Opsonized particles were subsequently stained with donkey anti-human secondary antibody conjugated to DyLight488 (Jackson ImmunoResearch). Homogeneity in opsonization and labeling was determined with a Canto II flow cytometer (BD Biosciences) equipped with 405-, 488-, and 633-nm lasers. Flow cytometry data analysis was performed with FlowJo software (Tree Star, Inc.).

Enzymatic Assay for Total PA Content—Cellular PA was measured enzymatically (32) using a total phosphatidic acid kit (Abnova, Taipei City, Taiwan) adhering to the manufacturer's instructions. In brief, lipids were purified from confluent RAW 264.7 macrophages grown on 10-cm diameter plates by methanol/chloroform extraction in polypropylene centrifuge tubes. Purified lipids were subjected to lipase digestion, and subsequently, glycerol-3-phosphate oxidase was used to produce H_2O_2 from glycerol 3-phosphate (a by-product of PA digestion by lipases). H_2O_2 was then reacted with 10-acetyl-3,7-dihydroxyphenoxazine in the presence of horseradish peroxidase to yield resorufin (Amplex Red). Resorufin fluorescence was detected using a SpectraMax Gemini EM microplate reader (Molecular Devices, Sunnyvale, CA). PA content was normalized to unit protein, which was in turn determined before lipid extraction by a bicinchoninic acid assay (Thermo Scientific, Rockford, IL).

Microscopy and Image Analysis—For fluorescence quenching experiments, coverslips were placed in a Leiden chamber maintained at 37 °C and mounted on the stage of a microscope (model DM IRB; Leica). The cells were excited by light from an XFO X-Cite 120 lamp (XFO Life Sciences Group) transmitted through a 485 ± 10-nm excitation filter directed to the sample using a 505-nm dichroic mirror and captured by a cooled charge-coupled device camera (Cascade II; Photometrics) using 2 × 2 binning. The filter wheel and camera were under the control of MetaFluor software (MDS Analytical Technologies). All other fluorescence images were acquired by spinning-disc con-

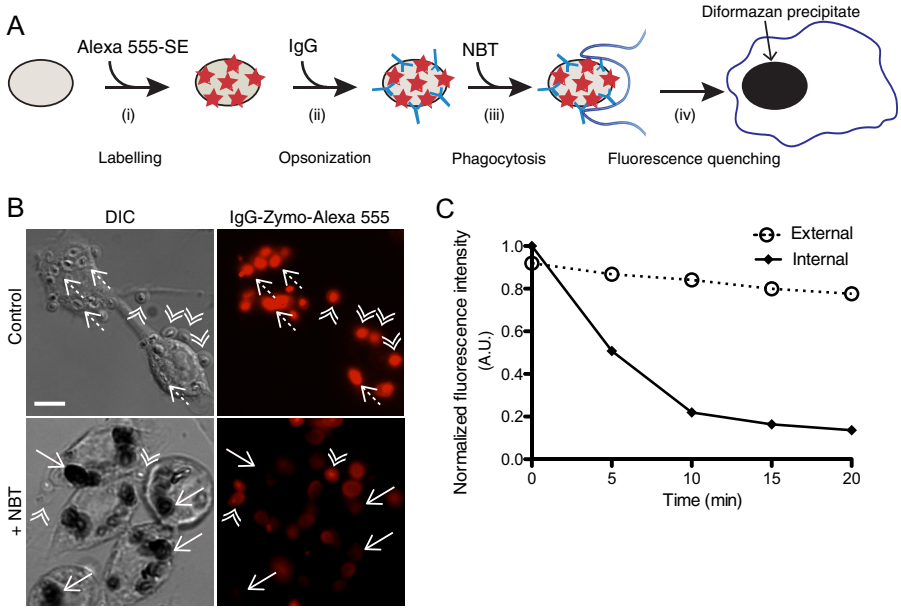

FIGURE 1. **Detection of superoxide production within individual phagosomes by NBT-mediated fluorescence quenching.** *A,* schematic of the experimental protocol. Zymosan particles labeled with Alexa 555-SE (*i*) and opsonized with human IgG (*ii*) were used as phagocytic targets for RAW macrophages in the presence of the membrane permeable dye NBT (*iii*). Uptake of opsonized, labeled zymosan (IgG-Zymo-Alexa 555) and the ensuing activation of NOX2 results in the generation of superoxide anions capable of reducing NBT to diformazan crystals in the phagosomal lumen. Diformazan precipitates in the form of blue/black deposits (*iv*) and effectively quenches the fluorescence signal emitted by the fluorescently labeled zymosan particles. *B,* representative differential interference contrast (*DIC, left panels*) and corresponding epifluorescence (*right panels*) images of RAW macrophages fixed 25 min after exposure to IgG-opsonized zymo-Alexa 555. Where indicated, cells were incubated with NBT prior to and throughout phagocytosis. *Double arrowheads* point to noninternalized particles, and diformazan-negative and -positive phagosomes are indicated by *dashed* or *solid arrows*, respectively. *Scale bar,* 5 μm. *C,* quantification of fluorescence intensity as a function of time during phagocytosis. *Open circles* and *closed diamonds* correspond to external and internalized IgG-Zymo-Alexa 555, respectively. Images in *B* and the results in *C* are representative of at least six and two individual experiments of each kind, respectively. ***, $p < 0.005$.

focal microscopy. The systems in use in our laboratory (Quorum) are based on a microscope (Axiovert 200 M; Carl Zeiss, Inc.) with ×63 or ×100 objectives and a ×1.5 magnifying lens. The units are equipped with diode-pumped solid-state lasers (440, 491, 561, 638, and 655 nm; Spectral Applied Research), a motorized XY stage (Applied Scientific Instrumentation), and a piezo focus drive. Images were acquired using back-thinned, electron-multiplied, or conventional cooled charge-coupled device cameras (Hamamatsu Photonics) driven by the Volocity software (version 4.1.1; PerkinElmer Life Sciences).

Statistical Analysis—Statistical parameters were determined using GraphPad Prism 5c software (GraphPad Software, Inc.). To assess significance of differences, all comparisons between means of matched groups were two-tailed unpaired *t* tests relying on the analysis routines built in GraphPad Prism.

RESULTS

Identification and Quantification of Superoxide Production within Single Phagosomes through NBT-mediated Fluorescence Quenching—We devised a fluorescence quenching assay (illustrated diagrammatically in Fig. 1*A*) to monitor NADPH oxidase activity continuously within single phagosomes. To this end, we took advantage of the previously described deposition of diformazan generated from NBT at sites of superoxide production (16). Direct measurement by bright-field microscopy of the changes in light absorbance caused by diformazan deposition is complicated by the absorbance and scattering contributed by the cells and by the phagocytic targets, which vary as the particles are engulfed. To circumvent these problems, zymosan particles were labeled with Alexa 555-succinimidyl ester. The resulting labeled particles (referred to hereafter as Zymo-Alexa 555) were opsonized with human IgG and used as phagocytic prey. Phagocytosis was performed in the presence of NBT, which is membrane-permeable and capable of traversing both the plasma and phagosomal membranes, effectively reaching the phagosomal lumen. Upon activation of NOX, intraphagosomal deposition of the black-purple diformazan effectively quenches the fluorescence emitted by labeled phagocytic targets, interfering with the passage of both excitation and emission of light (Fig. 1, *A* and *B*). The amount of remaining fluorescence is therefore inversely proportional to the cumulative activity of the NAPDH oxidase. This is illustrated in Fig. 1*C*; although the fluorescence of internalized particles decays rapidly, the fluorescence of particles that remain extracellular is largely unaffected, showing only a minimal decrease attributable to photobleaching. Accordingly, little fluorescence quenching was observed when labeled particles underwent phagocytosis in the absence of NBT (Fig. 1*B*). It is noteworthy that the Alexa Fluor 555 is stable, and its fluorescence is unaffected between pH 4 and 10 (17), enabling measuring superoxide production independently of phagosomal acidification. Together, these observations indicate that the quenching assay is a suitable continuous measure of the production of superoxide by individual phagosomes. This notion was validated using 10 μM diphenyleneiodonium, a potent inhibitor of the NADPH oxidase that precluded fluorescence quenching (Fig. 2, *A* and *B*).

NADPH Oxidase Activation Is Heterogeneous—By implementing the assay described above, we detected considerable

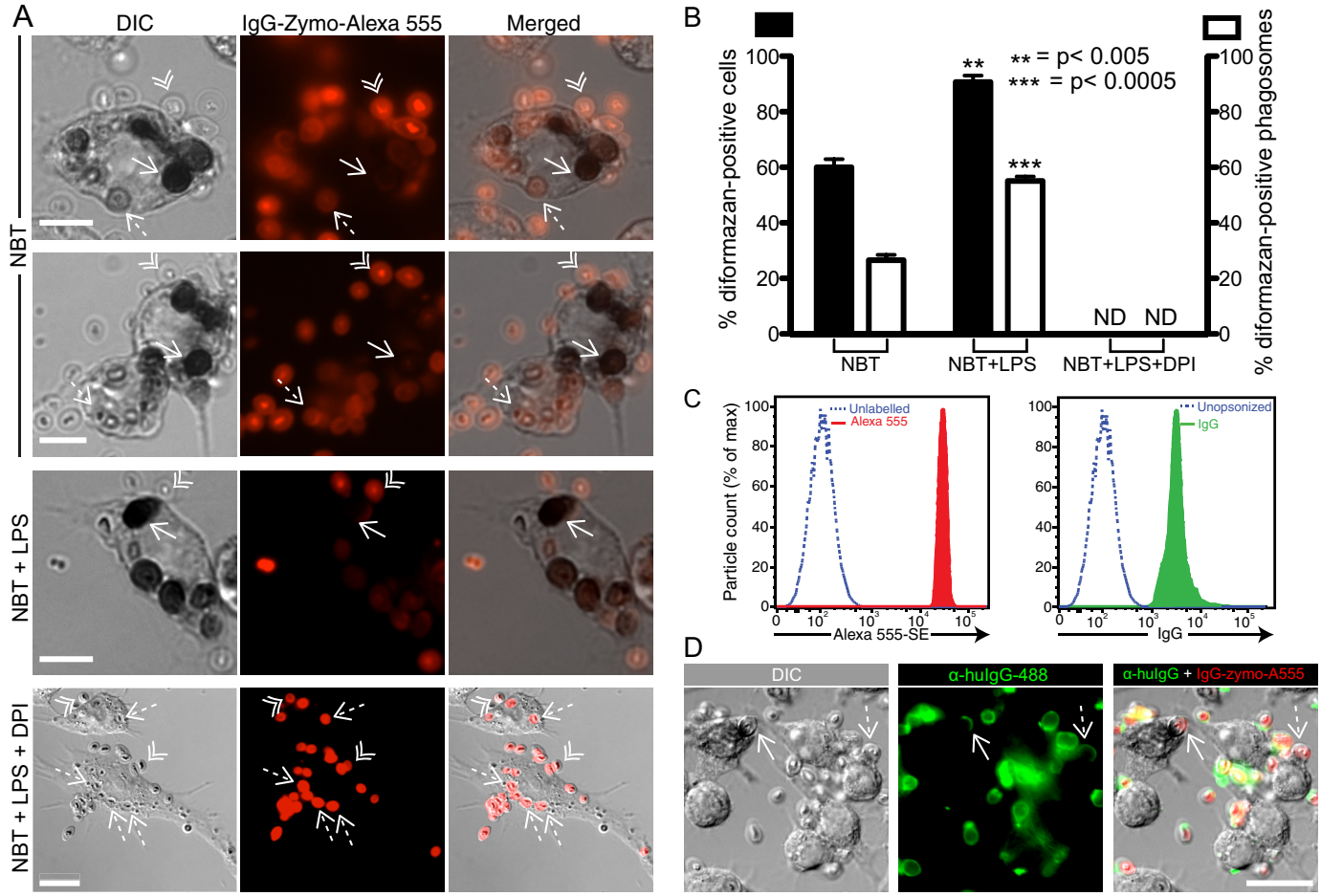

FIGURE 2. **Superoxide production during FcγR-mediated phagocytosis is heterogeneous.** *A,* representative DIC (*left panels*), corresponding epifluorescence (*middle panels*), and merged (*right panels*) images of RAW macrophages fixed 25 min after exposure to IgG-Zymo-Alexa 555 in the presence of NBT. The *top two panels* show differential diformazan deposition within phagosomes of single cells and between those of different cells. LPS-primed cells display a higher fraction of NOX2-responsive phagosomes and therefore reduced phagosomal heterogeneity, whereas exposure to the NOX inhibitor, diphenyleneiodonium (*DPI,* 10 μM), abrogates diformazan deposition and fluorescence quenching (*bottom panel*). The notation for *arrows* and *arrowheads* is as in Fig. 1. Images are representative of at least five independent experiments. *B,* quantification of the relative abundance of superoxide-producing cells (*left axis, black bars*) and phagosomes (*right axis, white bars*), before and after LPS activation or in the presence of diphenyleneiodonium, assessed as their ability to reduce NBT to its insoluble form and quench zymo-Alexa 555 fluorescence. Macrophages with at least one phagosome displaying deposits were classified as "positive cells." Data are averages ± S.E. of at least five individual experiments; a minimum of 80 phagosomes was counted per experiment. *C,* FACS histograms showing the homogeneity of Alexa 555 labeling (*left panel, red trace*) and IgG opsonization (*right panel, green trace*) of zymosan particles used as phagocytic targets. *D,* representative DIC (*left panel*), corresponding epifluorescence (*middle panel*), and merged (*right panel*) images showing differential superoxide production in two macrophages at an early stage of phagocytosis, preceding phagosomal sealing. Incompletely internalized IgG-Zymo-Alexa 555 particles were labeled with a DyLight488-conjugated antibody after fixing. Diformazan-positive and -negative phagosomes that are labeled by secondary antibody, and therefore unsealed and with equal access to extracellular NBT, are indicated with a *solid* and a *dashed arrow*, respectively. *Scale bars* in *A* and *D*, 5 μm.

heterogeneity in the responsiveness of individual phagosomes formed by RAW 264.7 macrophages (henceforth referred to as RAW). Remarkably, differences were noted not only between phagosomes in different cells but also among phagosomes formed by individual cells (Fig. 2*A*, *top two rows*), regardless of the time of phagosomal sealing. After a 30-min exposure to phagocytic targets, on average only 26 ± 1.9% of the phagosomes formed by each RAW cell displayed significant oxidase activity (Fig. 2*B*, *white bars*), whereas 60 ± 2.9% of the total macrophage population had at least one superoxide-generating phagosome (Fig. 2*B*, *black bars*).

We contemplated the possibility that either uneven labeling with Alexa 555 or variations in the degree of opsonization may have artifactually led to heterogeneity in the response measured. This possibility was discounted using flow cytometry. As illustrated in Fig. 2*C*, cytometric analyses of both zymosan particle labeling and opsonization yielded sharp, unimodal distributions that could not account for the observed heterogeneity in phagosomal oxidase activity.

Even though NBT is reportedly permeable across biological membranes (18), its rate of entry may be limiting. It is therefore conceivable that the observed heterogeneity in the NOX response reflects different amounts of NBT trapped in individual phagosomes at the time of sealing. To examine this possibility, we exposed RAW cells to IgG-Zymo-Alexa 555 in the absence of NBT for 7 min, an interval that allowed for the majority of particles to be internalized. Particles that had not been fully internalized by this time were labeled by addition of extracellular anti-human IgG labeled with DyLight488 and were thereby eliminated from further analysis. NBT was then added, and the reaction was allowed to proceed for a further 23 min (see Fig. 3*A* for a diagrammatic illustration of the protocol).

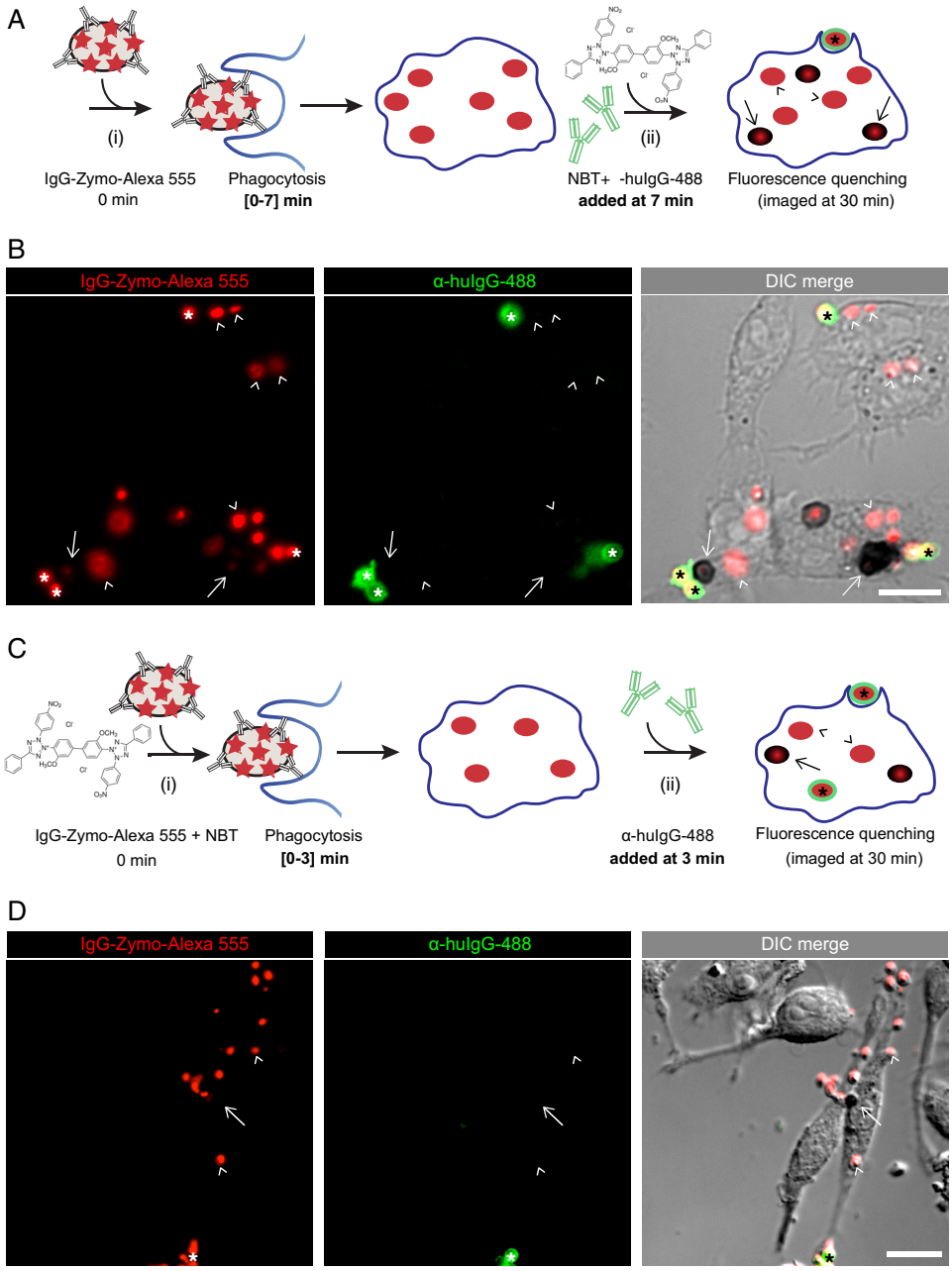

FIGURE 3. **Neither differential accumulation of NBT in individual phagosomes nor time-dependence of NOX can account for the observed phagosomal heterogeneity.** *A,* schematic of an experimental protocol designed to determine whether accessibility of NBT, the quenching agent, to phagosomal compartments is variable. RAW macrophages were challenged at 0 min with human IgG-opsonized zymosan particles labeled with Alexa 555-SE (IgG-Zymo-Alexa 555), and phagocytosis was allowed to continue for 7 min, at which point NBT was included in the reaction. A secondary 488 anti-human IgG was also added at this 7 min to mark phagocytic targets that had not been internalized at the time of first exposure of macrophages to NBT. Phagocytosis proceeded for an additional 23 min after addition of NBT, and cells were fixed at 30 min for imaging. *B,* representative epifluorescence (*left* and *middle panels*) and DIC (*right panel*) images of the experiment described in *A*. Phagocytic targets that fluoresce both in the *red* and *green channels* (indicated with an *asterisk*) had not yet been internalized at the time of NBT addition, whereas targets that emit only in the *red channel* had been engulfed prior to NBT addition. The *right panel* shows diformazan-positive targets (indicated with a *solid arrow*) and diformazan-negative targets (indicated with an *arrowhead*) that resided within sealed phagosomes in the same cell when the quenching dye was included in the reaction and thus had comparable access to NBT. *C,* schematic of an experimental protocol designed to determine whether time dependence of NOX could be responsible for phagosomal heterogeneity. Both NBT and IgG-Zymo-Alexa 555 were added to macrophages at 0 min, and phagocytosis was allowed to proceed for only 3 min before addition of a secondary 488 anti-human IgG to mark the 3-min time point. Phagocytosis then continued for an additional 27 min, and cells were image-fixed at 30 min. *D,* representative epifluorescence (*left* and *middle panels*) and DIC (*right panel*) images of the experiment are described in *C*. Phagocytic targets that fluoresce in the *red*, but not in the *green*, were internalized within the first 3-min window (out of a total 30 min). The *right panel* shows diformazan-positive and -negative phagocytic phagosomes that were internalized within said 3-min window and therefore had equivalent time intervals for phagosomal maturation and NOX activation. The notation for *asterisks, arrows,* and *arrowheads* is as in *A*. *Scale bars,* 10 μm.

Distinct heterogeneity in NOX activity was still observed among the phagosomes that had sealed prior to the addition of NBT (Fig. 3*B*). These data validate the notion that NBT can readily cross biological membranes and imply that differential trapping of NBT during sealing cannot explain the variability of the responses.

It is also worth noting that we routinely encountered nascent phagosomes that had not yet sealed. Some but not all of these displayed diformazan precipitates at the base of the forming cup (*e.g.* Fig. 2*D*). Because at this stage access to NBT is unhindered, the variable response cannot be attributed to insufficient exposure to NBT; it also rules out differential permeability of the phagosomal membrane to NBT as the source of the heterogeneity illustrated in Fig. 3*B*.

Finally, we considered the distinct possibility that the heterogeneity in superoxide production was a consequence of asynchrony of the phagocytic process and/or of the activation of the oxidase. To address this, RAW cells were allowed to ingest IgG-Zymo-Alexa 555 in the presence of NBT for 30 min, as in Figs. 1 and 2. However, in these experiments particles that had not been internalized after the first 3 min were marked by addition of a fluorescently labeled secondary antibody (see Fig. 3*C* for a diagrammatic illustration of the protocol). By excluding those targets that were ingested after addition of the antibody, we were able to analyze the response of only those phagosomes formed within a narrow time window, *i.e.* the initial 3 min; these were then allowed to mount an oxidative response for an additional 27 min. The integrated cumulative response over this comparatively long period should have minimized the consequences of the slight phagocytic asynchrony incurred during the initial 3 min. Notably, considerable heterogeneity was nevertheless recorded under these conditions (Fig. 3*D*). Jointly, these experiments imply that the variable responsiveness of the phagosomal oxidase is neither an artifact caused by uneven exposure to NBT nor a reflection of asynchrony. Instead, the oxidative response of phagosomes appears to be intrinsically heterogeneous.

It is widely accepted that bacterial endotoxin can robustly prime phagocytes for superoxide production (19), although the underlying mechanism is still incompletely understood (20). We sought to determine whether this reflects increased production of superoxide by a constant number of phagosomes or an increased fraction of responding phagosomes. Overnight incubation of RAW macrophages with the toll-like receptor-4 (TLR-4) agonist, lipopolysaccharide (LPS, 100 ng/ml), noticeably increased the fraction of phagosomes that mounted an effective respiratory burst from 26 ± 1.9 to 55 ± 1.6%, as well as the number of cells with responsive phagosomes from 60 ± 2.9 to 91 ± 2.3% (Fig. 2, *A* and *B*). Thus, priming reduced the heterogeneity of the respiratory response.

Assessment of the Roles of PtdIns(3,4,5)P_3, Phosphatidic Acid, and PtdIns(3)P in the Genesis of the Functional Heterogeneity—Several lipid intermediates are required for the initiation and progression of phagocytosis, including the deployment of the NADPH oxidase. Engulfment of large particles and completion of maturation require activation of class I phosphatidylinositol 3-kinases (21). Because different degrees of receptor engagement can influence the extent of PtdIns(3,4,5)P_3 generation (22), we analyzed whether differential production of this phosphoinositide accounted for the variable respiratory burst response. We used a genetically encoded biosensor, a chimeric construct consisting of the pleckstrin homology domain of Akt/PKB tagged with GFP, to monitor the formation of PtdIns(3,4,5)P_3 during the course of phagocytosis of IgG-opsonized zymosan. Spinning disc confocal microscopy was used to monitor translocation of the biosensor to the phagosomal membrane over time. Consistent with earlier findings (23), we could readily detect recruitment of PH-Akt-GFP to nascent and recently formed phagosomes, followed by rapid loss of the probe after sealing (Fig. 4*B*, *top*). Of note, virtually 100% of the phagosomes induced by IgG-zymosan accumulated the probe to a comparable degree (Fig. 4*C*). Thus, failure to generate PtdIns(3,4,5)P_3 cannot account for the inability of a considerable fraction of phagosomes to activate the NADPH oxidase.

A similar approach was used to evaluate the role of PA. In this instance, we used a probe composed of two tandem copies of the PA-binding domain of the yeast protein Spo20p, which has been used in the past to monitor PA distribution (10, 11). The PA probe (hereafter referred to as 2PABD-GFP), was optimized by adding a nuclear export signal N-terminally to the PABD domains, as the probe tends to partition to the nuclear compartment otherwise.[6] To ensure that this modification did not interfere with the ligand specificity of the probe, we monitored the distribution of 2PABD-GFP in HeLa cells before and after altering the PA content by pharmacological, biochemical, or enzymatic means. Unlike phagocytes (24), unstimulated HeLa cells have little PA in their plasma membrane. Exposure to exogenous PA (100 μM for 10 min) induced rapid association of 2PABD-GFP with the plasma membrane (supplemental video 2), validating the responsiveness of the probe. Recruitment of 2PABD-GFP to the membrane was also observed when HeLa cells were treated with 1 μM ionomycin for 2 min (supplemental video 3); calcium entering through this ionophore is known to activate phospholipase C, generating DAG, a precursor of PA generation by DGK. Moreover, recruitment of 2PABD-GFP was also observed when HeLa cells were co-transfected with wild-type PLD2, a plasma membrane-associated enzyme that converts phosphatidylcholine to PA (data not shown). Of note, expression of neither an inactive form of PLD2 nor of PLD1 (which is not found at the membrane and instead has a vesicular, punctate distribution) caused recruitment of the PA probe to the membrane. Jointly, these results provide evidence that the 2PABD biosensor utilized in this study is a suitable probe for PA.

In contrast to HeLa cells, a sizable amount of the PA probe was found to associate with the plasma membrane of unstimulated RAW macrophages. The bound probe was rapidly released to the cytosol when RAW cells were treated with the DGK inhibitor R59 022 (DGKi I, 30 μM), suggesting that PA is continuously synthesized by phosphorylation of DAG (supplemental video 4). Accordingly, addition of DGKi I caused a concomitant accumulation of DAG in the membrane of RAW cells (supplemental video 4) and a reduction in the cellular content of PA measured biochemically (Fig. 6*C*). It is worth noting that this assay cannot distinguish lyso-PA from diacylated PA, but the former is less abundant and is expected to contribute marginally to the determinations. These observations further validate the reliability of the 2PABD biosensor. Despite being present at the membrane of unstimulated cells, 2PABD-GFP

[6] F. Zhang and G. Du, manuscript in preparation.

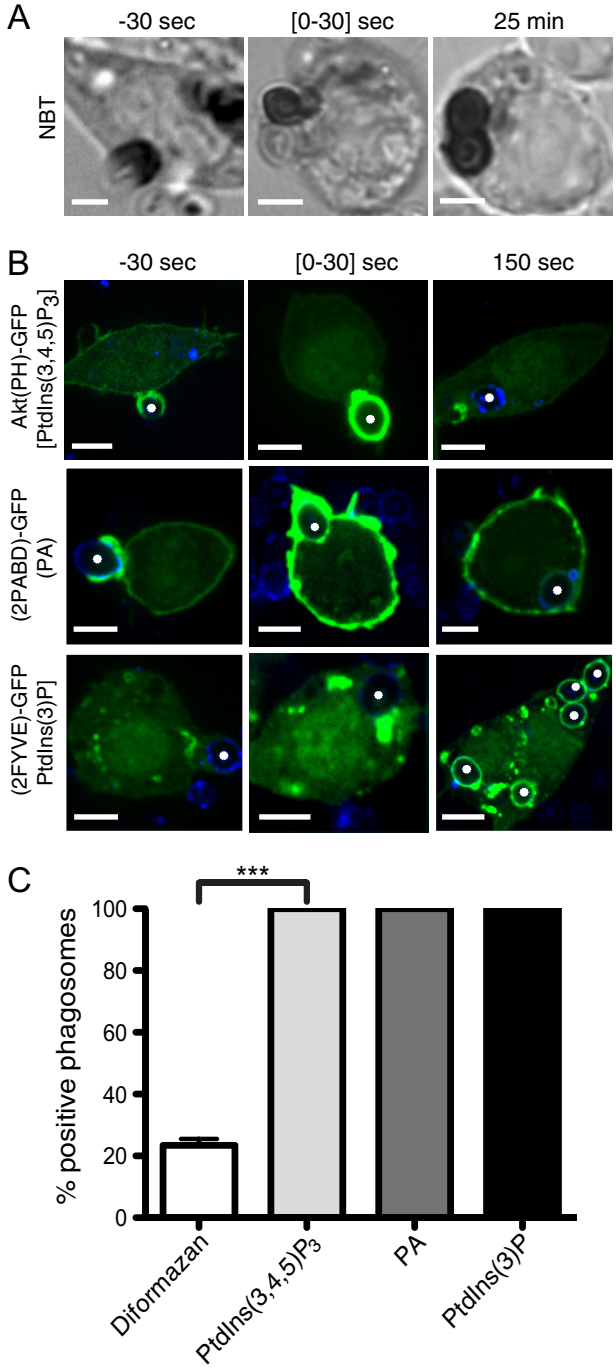

FIGURE 4. **Phagosomal population is uniformly endowed with PtdIns(3,4,5)P_3, PA, and PtdIns(3)P during the respiratory burst.** *A*, representative DIC images of live RAW macrophages during phagocytosis of IgG-opsonized zymosan in the presence of NBT. The phagocytosis time course is delineated to three stages as follows: pseudopod extension (minus 30 s, *left panel*), phagosome sealing (0–30 s, *middle panel*), and phagosome maturation (plus 25 min, *right panel*). *B,* spinning disk confocal fluorescence images of RAW macrophages challenged with IgG-opsonized zymosan particles labeled with Cy5-conjugated secondary antibody (*blue*). Cells were transfected with constructs encoding fluorescently tagged domains that served as biosensors for PtdIns(3,4,5)P_3 (Akt(PH)-GFP, *top panel*), PA (2PABD-GFP, *middle panel*), and PtdIns(3)P (2FYVE-GFP, *bottom panel*). Recruitment of the probes to the phagosomal membrane was monitored during pseudopod extension (minus 30 s), phagosome sealing (0–30 s), and early stages of maturation (plus 150 s). *Asterisks* indicate phagosomes. Note that the −30-s image for PA was underexposed compared with the other times, to avoid saturation of the fluorescence accumulated at the cup. *Scale bars* in *A* and *B*, 5 μm. *C,* quantification of the fraction of phagosomes displaying formazan deposits and accumulation of PtdIns(3,4,5)P_3, PA, or PtdIns(3)P. Data indicate the average fraction of positive phagosomes per cell for each condition at the following time points: diformazan (20 min after exposure to zymosan); PtdIns(3,4,5)P_3 (0–30 s after phagosome sealing); PA (30 s before phagosome sealing); PtdIns(3)P (150 s after sealing). Data are representative of at least five independent experiments; a minimum of 100 phagosomes was counted per experiment.

accumulated further at the phagocytic cup (Fig. 4*B*, *middle*). The accumulation dissipated rapidly after phagosome closure, with PA being only marginally detectable in the phagosomal membrane 3 min after sealing. As in the case of PtdIns(3,4,5)P_3, essentially all phagosomes analyzed accumulated considerable amounts of PA, judged by the recruitment of the Spo20p probe (Fig. 4*C*). Therefore, the inability of a large fraction of phagosomes to form superoxide cannot be attributed to lack of PA accumulation.

PtdIns(3)P, a product of the class III phosphatidylinositol 3-kinase, was recently shown to be required for phagosomal superoxide generation, likely by recruitment of the $p40^{phox}$ subunit of the oxidase via its PX domain (25). A probe based on the FYVE domain of EEA1 was used to quantify the fraction of phagosomes that accumulate PtdIns(3)P. As described before (2, 26), PtdIns(3)P was not detectable at the phagosomal cup and was only observable ≥1 min after sealing, persisting for nearly 10 min at the phagosomal membrane. Two lines of evidence suggest that PtdIns(3)P is not responsible for the heterogeneous respiratory burst. First, as for the two other lipids, PtdIns(3)P was found in every phagosome studied (Fig. 4, *B* and *C*). Second, PtdIns(3)P is seen 2–5 min post-phagosome sealing, at which time heterogeneity is already observed. Moreover, as illustrated in Fig. 4*A* and supplemental video 1, diformazan deposits initially form at the base of the cup, preceding phagosome closure (see also Fig. 2*D*). Even at this stage, heterogeneity is readily apparent. This excludes PtdIns(3)P, which forms only later and is likely important for the maintenance but not the initiation of the response, as the source of the variable respiratory burst. Jointly, these results suggest that neither PtdIns(3,4,5)P_3, PA, nor PtdIns(3)P are responsible for the heterogeneous activation of the NADPH oxidase during IgG-mediated phagocytosis.

Diacylglycerol Heterogeneity Correlates with NADPH Oxidase Activity—DAG stimulates conventional and novel PKC isoforms (27, 28) that phosphorylate and activate the cytosolic components of the NOX complex (29–31). We therefore hypothesized that variations in the phagosomal content of DAG could account for the observed fluctuations in superoxide production. To test this hypothesis, we monitored DAG dynamics using a genetically encoded biosensor consisting of the C1 domain of PKCδ fused to GFP. Remarkably, this probe was recruited to some but not all the phagosomes (Fig. 5*A*); heterogeneity was observed not only across cells, but also between phagosomes formed by individual cells. In otherwise untreated macrophages, only 26 ± 2.5% of the phagosomes induced by IgG-coated zymosan were visibly endowed with DAG. In contrast, overnight activation of macrophages with LPS (100 ng/ml) increased the fraction of DAG-positive phagosomes to 60 ± 2.6% (Fig. 5*B*). Of note, the fraction of phagosomes displaying measurable NADPH oxidase activity (Fig. 5*C*)

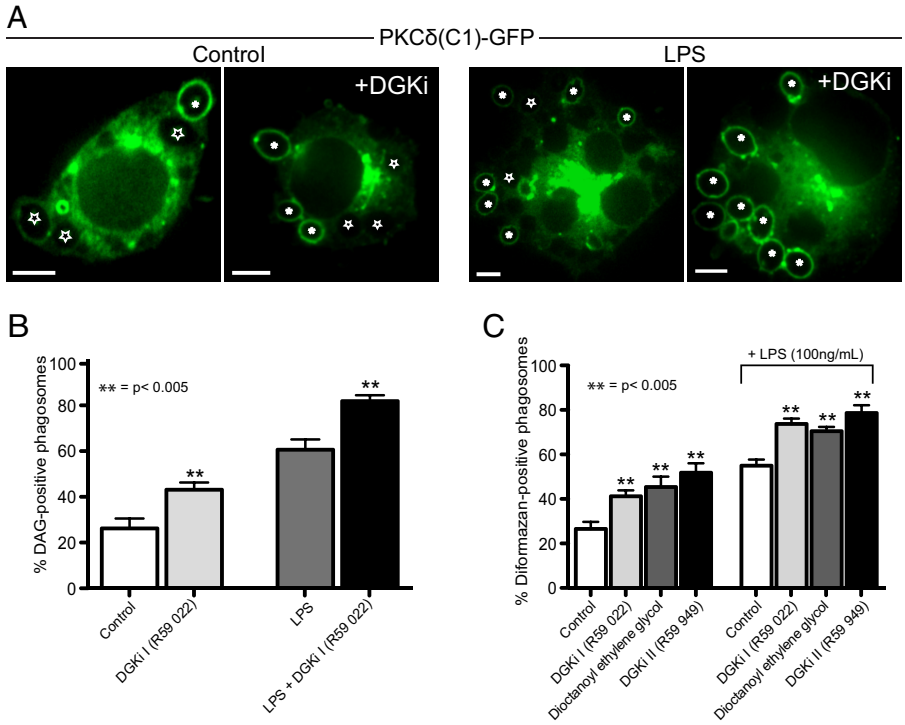

FIGURE 5. **Diacylglycerol is heterogeneously distributed across the phagosomal population in a manner that mirrors NADPH activity.** *A*, representative spinning disk confocal fluorescence images of RAW cells transfected with a diacylglycerol biosensor, acquired during engulfment of IgG-opsonized zymosan particles. Where indicated, cells were incubated for 20 min prior to phagocytosis with 30 μM of the diacylglycerol kinase inhibitor, R59 022 (DGKi I), and/or primed overnight with LPS (0.1 μg/ml). Diacylglycerol-positive and -negative phagosomes are indicated with *asterisks* or *stars*, respectively. *Scale bars,* 5 μm. Quantification of the relative abundance of diacylglycerol-positive (*B*) and diformazan-positive (*C*) phagosomes after DAG kinase inhibition, LPS priming, or both. DAG kinases were inhibited with either R59 022, R59 949, or dioctanoyl ethylene glycol. Data are averages ± S.E. of positive phagosomes per cell for each condition, 5 min after exposure to zymosan. Data are representative of at least five independent experiments; a minimum of 100 phagosomes was counted per experiment.

correlated closely with the fraction of DAG-positive phagosomes for both untreated and LPS-activated macrophages (Fig. 5, *A* and *B*).

Although the correlation between formation of DAG and activation of the oxidase is striking, it does not necessarily imply a causal relationship. To more directly test whether the variability in DAG accumulation is responsible for the heterogeneous respiratory burst, we sought to alter the DAG content of forming phagosomes. During phagocytosis, DAG is detected only fleetingly (≤1 min) on the phagosomal membrane, as it is quickly metabolized, at least in part, by conversion to PA, a reaction catalyzed by DAG kinase (DGK) family members. This is consistent with the observations reported in Fig. 4*B*, where PA was found to accumulate in forming phagosomes. Thus, in principle, inhibition of DGK activity would be expected to enhance the phagosomal accumulation of DAG. This notion was tested by pretreating RAW macrophages with 30 μM DGKi I for 20 min prior to the initiation of phagocytosis. Exposure to DGKi increased the average number of diacylglycerol-positive phagosomes from 26 ± 2.5 to 43 ± 1.9% in otherwise untreated cells, and it further increased the number of positive phagosomes to 82 ± 1.5% in LPS-activated cells (Fig. 4*B*). Notably, the changes in DAG content were paralleled by variation in NOX activity (Fig. 5*C*); stabilization of DAG by pharmacologically inhibiting DGK enhanced superoxide production and reduced the heterogeneity of the NOX response among phagosomes formed by both control (non-LPS treated) and LPS-activated cells. To verify whether the effects of DGKi I were indeed caused by inhibition of DGK, we used two additional inhibitors of this enzyme, R59 949 (DGKi II) and the structurally unrelated dioctanoyl ethylene glycol, a nonphosphorylatable DAG analog. Both of these compounds decreased the cellular content of PA to an extent similar to that described for DGKi I, as measured biochemically (Fig. 6*C*). More importantly, DGKi II and dioctanoyl ethylene glycol recapitulated the enhanced NOX responsiveness induced by DGKi I in otherwise untreated and in LPS-treated macrophages (Fig. 5*C*). These results suggest that one or more DAG kinase isoforms antagonize NOX activation by terminating DAG signaling. That DAG is in fact converted to PA during phagocytosis was documented in RAW cells expressing 2PABD-GFP. In parallel with the accumulation of phagosomal DAG, inhibition of DGK activity caused a marked decrease in the PA content of the phagosomal membrane (Fig. 6, *A* and *B*).

Expression of Diacylglycerol Kinase Isoforms in Macrophages—The preceding pharmacological experiments imply that one or more DGK isoforms are present and active on the membranes of macrophages. The endogenous expression of DGK in RAW cells was verified by RT-PCR. Messages for all isoforms (α through κ) were found to be expressed by RAW cells (Fig. 7*A*). The subcellular distribution of representative members of all five DGK subfamilies was next analyzed by confocal microscopy. Because specific antibodies to each of the isoforms are not available, macrophages were instead transfected with con-

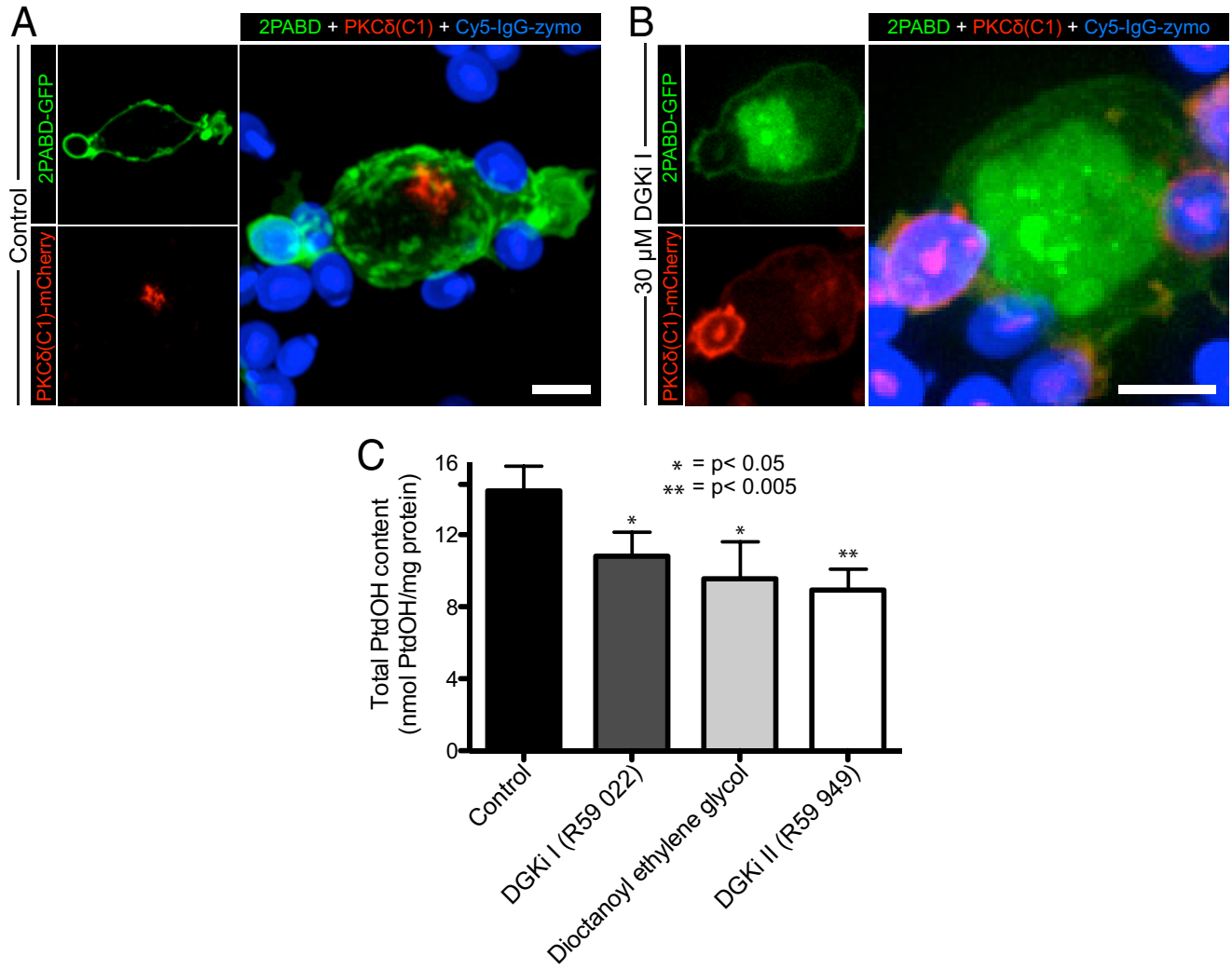

FIGURE 6. **PA content of macrophages is controlled by DGKs.** *A* and *B,* representative spinning disk confocal fluorescence sections (*left panels*) and multichannel Z projection (*right panel*) of RAW cells co-transfected with 2PABD-GFP (PA probe) and PKCδ(C1)-mCherry (DAG probe) during phagocytosis of IgG-opsonized zymosan particles (labeled with a Cy5-conjugated secondary antibody, shown in *blue*). Under control conditions (*A*), the PA probe localizes primarily to the plasmalemma and acutely accumulates at the phagosomal membrane as the phagosome seals; the DAG probe remains primarily restricted to juxtanuclear compartments. Conversely, treatment with 30 μM DGKi I (*B*) induces dissociation of the PA probe from plasma and phagosomal membranes and the concomitant recruitment of the DAG probe to these compartments. *Scale bars,* 5 μm. *C,* quantification of total PA from cell lysates, as determined using the enzymatic assay described under "Experimental Procedures." Lysates were prepared from RAW macrophages that were either untreated (control) or were pretreated for 15 min with 30 μM of DGK inhibitors I or II (R59 022 or R59 949, respectively) or 100 μM of dioctanoyl ethylene glycol. Data are means ± S.E. of the total cellular PA content (in nmol/mg of protein). Three independent experiments were performed per condition.

structs encoding the individual GFP-tagged DGKs; the translocation of the chimeric DGKs to sites of phagocytosis was then evaluated by addition of IgG-opsonized zymosan particles. The α, γ, and ϵ isoforms were primarily cytosolic and did not show particular accumulation at sites of phagosome formation. DGKδ-GFP appeared as punctate structures, which may have been homotypic aggregates caused by heterologous (over)expression. The γ, θ, and ζ isoforms could be detected at the plasmalemma, albeit modestly, and their concentration did not increase at sites of phagocytosis. These isoforms were not investigated further. In contrast, DGKβ was exclusively membrane-bound in unstimulated cells. Remarkably, in the course of particle engulfment, this isoform accumulated at the base of the phagocytic cup and in extending pseudopods (Fig. 7*B*, *top row, middle panel*, and supplemental video 5).

Modulation of NOX Responsiveness through DGKβ-mediated Control of Phagosomal DAG Signaling—We took advantage of the preferential accumulation of DGKβ in forming phagosomes to test the notion that DAG availability limits the generation of superoxide during particle ingestion. We postulated that the forcible (over)expression of DGKβ would effectively deplete phagosomal DAG, and consequently diminish superoxide generation by nascent phagosomes. A representative experiment is illustrated in Fig. 8, *A–C*, where RAW cells were co-transfected with the DAG probe, PKCδ(C1)-mCherry, and either wild-type or kinase dead (KD(G495D)) DGKβ-GFP. Note that phagocytosis proceeded in the presence of both wild-type and kinase-dead DGKβ. Remarkably, very few of the phagosomes accumulated DAG in cells expressing wild-type DGKβ (Fig. 8, *A* and *C*). Conversely, most of the phagosomes accumulated

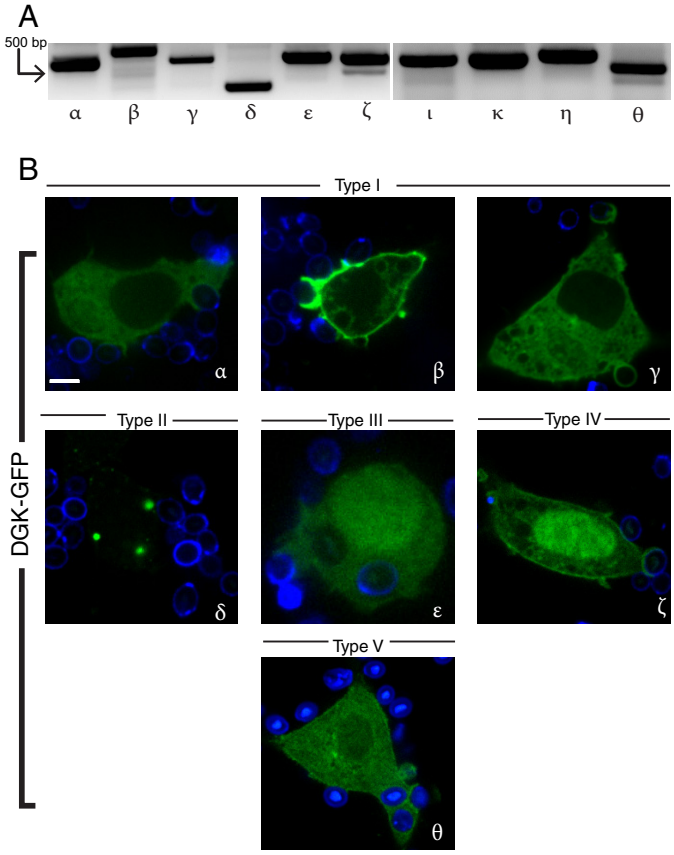

FIGURE 7. **Transcription and subcellular distribution of DGK isoforms.** *A,* endogenous transcript expression of distinct DGK isoforms (α through κ). Total mRNA was purified from RAW cells, and DGK isoform expression was detected by RT-PCR using transcript-specific primers encompassing exon-exon junctions. All amplicon sizes were as predicted by primer design. *B,* subcellular distribution of the indicated GFP-tagged DAG kinase isoforms, representing the five DGK families, during phagocytosis of IgG-opsonized zymosan targets (labeled with a Cy5-conjugated secondary antibody, shown in *blue*). *Scale bars,* 5 μm. Images in *B* are representative of at least five independent experiments.

DAG in cells expressing the kinase-dead DGKβ (Fig. 8, *B* and *C*), which may have exerted a dominant-negative effect.

That DAG formation is limiting to superoxide generation was documented by the experiments shown in Fig. 8, *D–F*, where diformazan deposition was quantified in cells expressing excess wild-type or kinase-dead DGKβ, as well as in control cells. The overexpression of wild-type DGKβ led to a reduction in superoxide production from 23 ± 2.0 to 7.0 ± 1.1% in otherwise untreated cells, and from 58 ± 1.2% to 9 ± 1.2% in LPS-primed cells (Fig. 8*F*). In contrast, expression of kinase-dead DGKβ increased the proportion of NOX-responsive phagosomes to 49 ± 2.4% in otherwise untreated cells and to 71 ± 2.4% in LPS-primed cells.

Cumulatively, our results indicate that the extent of DAG accumulation varied among phagosomes, accounting for the heterogeneity in the oxidative response, and that DGK modulates NOX activation by curtailing the accumulation of DAG, converting it to PA.

DISCUSSION

It is commonly assumed that all phagosomes formed by a defined, homogeneous target particle have the same composition, trigger identical signals, and therefore undergo comparable maturation pathways (33). Nonetheless, emerging evidence suggests that even when generated by an identical ligand-receptor combination, phagosomes are heterogeneous. Unappreciated variation in the density or disposition of ligands on the particle surface and/or in the distribution or responsiveness of receptors on the phagocyte membrane can result in the formation of phagosomes with different properties (22). To understand the source and significance of this heterogeneity, it is imperative to analyze the behavior of single phagosomes, as opposed to the more conventional population assays. Even flow cytometric data describing the behavior of individual cells can be inadequate, inasmuch as multiple phagosomes often co-exist in a single cell. These considerations prompted us to develop an assay to dynamically study the development of the respiratory burst in individual phagosomes. Pre-existing methods to analyze superoxide generation in phagosomes had limitations. Those that use soluble detectors, such as luminol, C11-BODIPY, or cytosolically trapped fluorogenic probes like dihydrofluorescein, are unable to distinguish oxidants generated at the plasmalemma from those formed by phagosomes, cannot detect single phagosomes, and in most cases, the nature of the oxidant detected is unclear, making the measurements liable to extraneous factors such as the presence of peroxidases (20). Reagents like OxyBURST, which can be attached covalently to the phagocytic particle, can in principle be used to monitor the behavior of single phagosomes. However, this approach has several shortcomings as follows: not only is the oxidation of the precursor sensitive to peroxidases, but also the resulting fluorescence is sensitive to pH and highly susceptible to photobleaching (36). More importantly, the amount of the probe bound to the particle is finite, compromising the sensitivity and linearity of the measurements over extended periods, particularly in phagosomes with high rates of oxidant production.

We circumvented these methodological limitations by designing a novel fluorescence-quenching assay that relies on NBT, which is converted to insoluble diformazan at sites of superoxide production. Because NBT readily traverses biological membranes and its availability is not limiting, the deposition of diformazan can in principle proceed linearly for indefinite periods. Indeed, NBT has been used extensively to monitor superoxide generation in a variety of systems (18, 37, 38). However, to our knowledge, it had not been applied to the quantitative measurement of single phagosomes, in all likelihood because it is difficult to discern the absorbance of diformazan from the light absorbed or scattered by the particle and by the phagocyte itself. We overcame this limitation by using fluorescently labeled particles and measuring quenching of their fluorescence, rather than the absorbance of NBT. Labeling the phagocytic targets with a bright photo-resistant and pH-insensitive fluorophore (Alexa Fluor 555) enabled accurate measurements over extended periods. In this manner, we were able to monitor superoxide generation dynamically and unambiguously in single phagosomes. Application of this assay led us to appreciate and quantify the inherent heterogeneity of the respiratory response of phagosomes challenged with a seemingly homogeneous particle. Variability in the response has been noted between cells, as well as between phagosomes of a particular cell. Cell-to-cell heterogeneity in the respiratory burst was

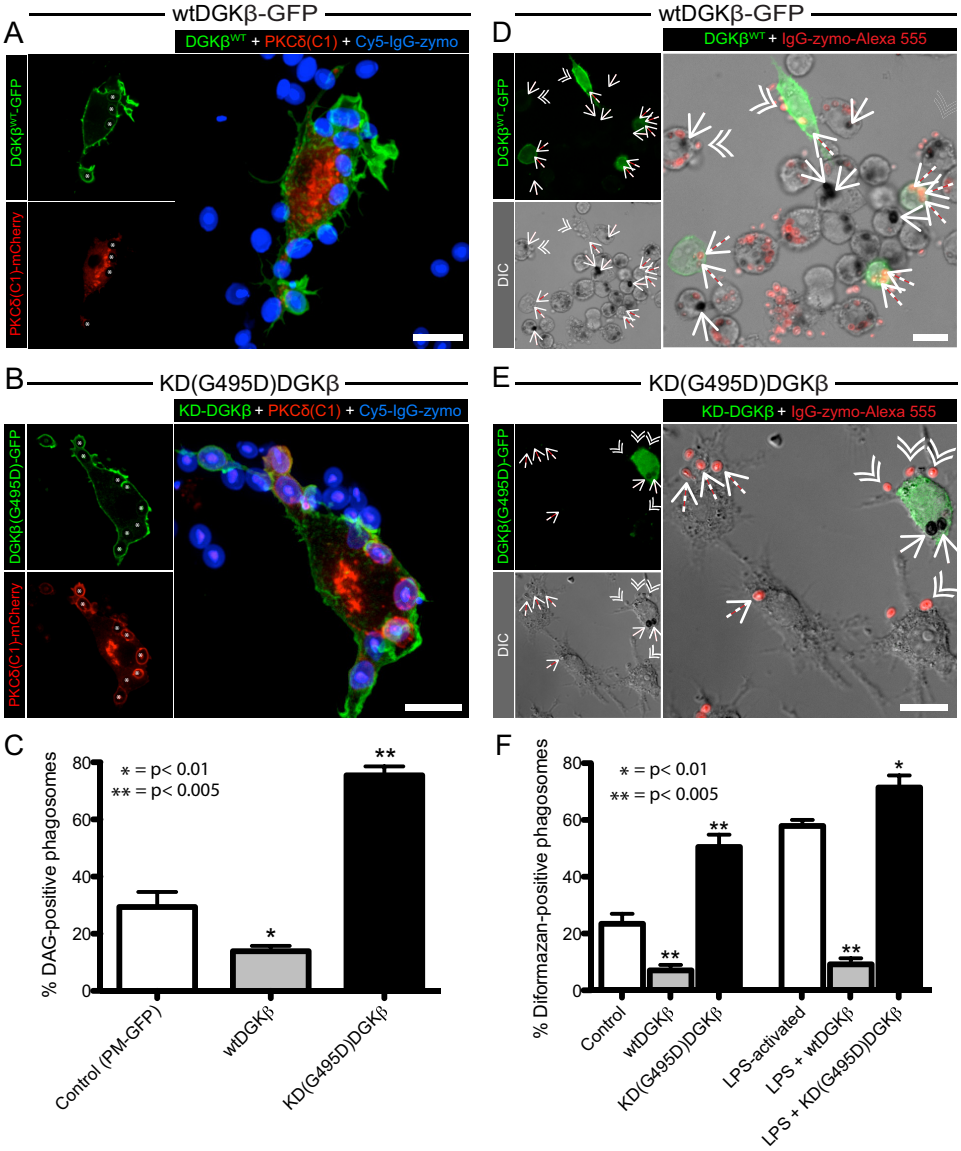

FIGURE 8. **Modulation of NOX activity through diacylglycerol kinase β-mediated control of phagosomal DAG.** *A* and *B,* representative confocal sections (*left panels*) and multichannel Z projection (*right panels*) of RAW cells co-transfected with PKCδ(C1)-mCherry (DAG probe) and either (*A*) wild-type (*wt*) or (*B*) kinase-dead (KD(G495D)) DGKβ-GFP during phagocytosis of IgG-opsonized zymosan particles (labeled with a Cy5-conjugated secondary antibody, shown in *blue*). *Asterisks* indicate phagosomes. *Scale bars,* 10 μm. *C,* quantification of the portion of phagosomes endowed with DAG in RAW cells expressing either wild-type or kinase-dead DGKβ relative to control cells transfected with the plasma membrane marker PM-GFP. Data are averages ± S.E. of positive phagosomes per cell for each condition, 3 min after exposure to zymosan. At least three independent experiments were performed and 80 phagosomes counted for each condition. *D* and *E,* representative epifluorescence and DIC (*left panels*) and merged (*right panel*) images of RAW cells transfected with either (*D*) wild-type or (*E*) kinase-dead DGKβ-GFP during phagocytosis of IgG-opsonized zymosan labeled with Alexa 555-SE (shown in *red*). RAW cells were fixed and imaged 25 min after exposure to NBT and IgG-opsonized Zymo-Alexa 555. *F,* quantification of data from experiments shown in *D* and *E*. Data are averages ± S.E. of diformazan-positive phagosomes per cell for each condition, 30 min after exposure to zymosan. At least three independent experiments were performed, and 60 phagosomes counted for each condition.

described earlier (40), and phagosome-to-phagosome differences were parenthetically reported for PLB-985 cells (41), but the source of this variability had not been defined.

In an effort to establish the source of the heterogeneity, we turned our attention to key bioactive lipids that are critical for mounting the respiratory burst. Phosphoinositides are of particular importance to the activation of the oxidase. The PX domain of $p40^{phox}$ selectively binds to PtdIns(3)P, and this interaction is most likely required for sustaining superoxide production in phagosomes (25, 42). In contrast, the PX domain of $p47^{phox}$ binds to PtdIns(3,4)P_2 and PtdIns(3,4,5)P_3 (31). This domain is unusual in that in contains two distinct lipid-binding pockets, allowing it to simultaneously and cooperatively bind to a phosphoinositide and a second small lipid such as PA (43). Thus, it has been postulated that by sensing multiple inputs, $p47^{phox}$ acts as a master integrator of PI3K and PLD signaling (29). We hypothesized that variations in the metabolism of these bioactive lipids could underlie the observed heterogeneity in NOX activity across the phagosomal population. However, although only a subpopulation of the phagosomes produced detectable amounts of superoxide, virtually all of them recruited comparable levels of the PtdIns(3,4,5)P_3, PtdIns(3)P, and PA biosensors (Fig. 4). We cannot rule out that subtle differences in the levels of these mediators contribute to the het-

erogeneity, but our measurements provided no evidence to this effect. Although it has been suggested that phagosomes are unevenly endowed with PtdIns(3)P (33), such heterogeneity was reported to become apparent 20 min after particle engulfment, long after the NOX complex is initially activated. Indeed, our observations indicate that the phagocytic oxidase is activated, and heterogeneously so, even prior to phagosome sealing (Figs. 2*D* and 3*A* and supplemental video 1).

In contrast to the consistent behavior and relatively long lasting presence of PA and the phosphoinositides, we found the incidence of DAG to vary greatly, both across phagosomes in different cells and within single cells. Of note, previous studies have conclusively demonstrated that DAG is a known activator of PKC signaling and hence of NOX assembly (7). Together, these observations led us to hypothesize that modulation of DAG production in phagocytes would have reciprocal effects on the observed heterogeneity in NOX responsiveness. Indeed, interfering with PKC or DAG signaling has profound effects on superoxide production at the cell population level in resident macrophages of the central nervous system (microglia) (44). The latter observation suggests that heterogeneity in phagosomal DAG signaling is a universal phenomenon for phagocytes and that DAG metabolism can be finely tuned according to the context of the immunological stimuli.

To elucidate whether DAG is in fact responsible for the heterogeneous activation of the NADPH oxidase, we utilized a combination of pharmacological and molecular biological methods. Given the redundancy in the number of DGKs and potential masking effects that could arise when knocking down any particular DGK isoform, we utilized DGK inhibitors to potentiate the accumulation of phagosomal DAG. Impairment of DGK activity not only augmented overall superoxide generation, it also reduced the heterogeneity of the response, facilitating the activation of phagosomes that would otherwise remain inactive. Similar effects were noted when expressing a kinase-dead DGKβ. Conversely, overexpression of functional DGKβ diminished the content of phagosomal DAG and, more significantly, reduced the fraction of responsive phagosomes. Jointly, these findings indicate that limiting amounts of DAG can account for the variable response of the NADPH oxidase in phagosomes.

Experiments using cells primed with bacterial endotoxin (LPS) are also consistent with this conclusion. Prior exposure to LPS is known to dramatically augment NOX activity (45). We complemented these observations by demonstrating that heterogeneity diminishes in parallel, as the fraction of unresponsive phagosomes was greatly reduced in LPS-treated macrophages and diminished even further upon treatment with DGKi (Figs. 2 and 5). The elevated responsiveness was accompanied by an increased fraction of DAG-positive phagosomes and a more intense and prolonged recruitment of PKCδ(C1), the DAG biosensor. The mechanism behind LPS priming of NOX could thus be attributed, at least partly, to an increase in the levels of the second messenger, DAG.

The phagosomal NADPH oxidase has been reported to remain active for ~30 min (20), although DAG is detectable on phagosomes only during the first minor two following particle engagement (46). DAG therefore seems to be essential for initiation of the response but not for its maintenance. The latter role may be served by PtdIns(3)P, which was shown to be involved in the recruitment of $p40^{phox}$ and in supporting superoxide formation in sealed phagosomes (25, 33).

In summary, we demonstrate that variable DAG production is associated with, and can account for, the heterogeneous nature of the respiratory burst. Rather than insufficient DAG generation, it appears that rapid conversion to PA by DGK precludes DAG accumulation in all phagosomes. This suggests that DGKs may operate as regulatory nodes in the signaling pathways leading to NOX activation. In this regard, it is interesting that DGK activity is significantly impaired in neutrophils from patients with localized juvenile periodontitis, which have elevated DAG levels and mount exaggerated oxidative responses (47). DGKs have been implicated in a variety of immunomodulatory processes, including attenuation of cytokine production in mast cells (48), down-regulation of T-cell receptor signaling (49), and the induction of anergic and tolerogenic profiles in lymphocytes (34, 35, 39). Our observations indicate that DGKs play an analogous immunoregulatory role in macrophages by executing the critical function of balancing effective microbicidal activity while preventing excessive generation of potentially harmful reactive oxygen species.

REFERENCES

1. Kamen, L. A., Schlessinger, J., and Lowell, C. A. (2011) Pyk2 is required for neutrophil degranulation and host defense responses to bacterial infection. *J. Immunol.* **186,** 1656–1665
2. Yeung, T., Ozdamar, B., Paroutis, P., and Grinstein, S. (2006) Lipid metabolism and dynamics during phagocytosis. *Curr. Opin. Cell Biol.* **18,** 429–437
3. Aratani, Y., Kura, F., Watanabe, H., Akagawa, H., Takano, Y., Suzuki, K., Dinauer, M. C., Maeda, N., and Koyama, H. (2002) Relative contributions of myeloperoxidase and NADPH oxidase to the early host defense against pulmonary infections with *Candida albicans* and *Aspergillus fumigatus*. *Med. Mycol.* **40,** 557–563
4. Casbon, A.-J., Allen, L.-A., Dunn, K. W., and Dinauer, M. C. (2009) Macrophage NADPH oxidase flavocytochrome B localizes to the plasma membrane and Rab11-positive recycling endosomes. *J. Immunol.* **182,** 2325–2339
5. Qualliotine-Mann, D., Agwu, D. E., Ellenburg, M. D., McCall, C. E., and McPhail, L. C. (1993) Phosphatidic acid and diacylglycerol synergize in a cell-free system for activation of NADPH oxidase from human neutrophils. *J. Biol. Chem.* **268,** 23843–23849
6. He, R., Nanamori, M., Sang, H., Yin, H., Dinauer, M. C., and Ye, R. D. (2004) Reconstitution of chemotactic peptide-induced nicotinamide adenine dinucleotide phosphate (reduced) oxidase activation in transgenic COS-phox cells. *J. Immunol.* **173,** 7462–7470
7. Cheng, N., He, R., Tian, J., Dinauer, M. C., and Ye, R. D. (2007) A critical role of protein kinase Cδ activation loop phosphorylation in formyl-methionyl-leucyl-phenylalanine-induced phosphorylation of p47(phox) and rapid activation of nicotinamide adenine dinucleotide phosphate oxidase. *J. Immunol.* **179,** 7720–7728
8. Regier, D. S., Waite, K. A., Wallin, R., and McPhail, L. C. (1999) A phosphatidic acid-activated protein kinase and conventional protein kinase C isoforms phosphorylate p22(phox), an NADPH oxidase component. *J. Biol. Chem.* **274,** 36601–36608
9. Griffiths, G. (2004) On phagosome individuality and membrane signalling networks. *Trends Cell Biol.* **14,** 343–351
10. Zeniou-Meyer, M., Zabari, N., Ashery, U., Chasserot-Golaz, S., Haeberlé, A.-M., Demais, V., Bailly, Y., Gottfried, I., Nakanishi, H., Neiman, A. M., Du, G., Frohman, M. A., Bader, M.-F., and Vitale, N. (2007) Phospholipase D1 production of phosphatidic acid at the plasma membrane promotes exocytosis of large dense-core granules at a late stage. *J. Biol. Chem.* **282,**

21746–21757
11. Du, G., and Frohman, M. A. (2009) A lipid-signaled myosin phosphatase surge disperses cortical contractile force early in cell spreading. *Mol. Biol. Cell* **20,** 200–208
12. Yeung, T., Terebiznik, M., Yu, L., Silvius, J., Abidi, W. M., Philips, M., Levine, T., Kapus, A., and Grinstein, S. (2006) Receptor activation alters inner surface potential during phagocytosis. *Science* **313,** 347–351
13. Flannagan, R. S., and Grinstein, S. (2010) The application of fluorescent probes for the analysis of lipid dynamics during phagocytosis. *Methods Mol. Biol.* **591,** 121–134
14. Shindo, M., Irie, K., Masuda, A., Ohigashi, H., Shirai, Y., Miyasaka, K., and Saito, N. (2003) Synthesis and phorbol ester binding of the cysteine-rich domains of diacylglycerol kinase (DGK) isozymes DGKγ and DGKβ are new targets of tumor-promoting phorbol esters. *J. Biol. Chem.* **278,** 18448–18454
15. Ota, T., Suzuki, Y., Nishikawa, T., Otsuki, T., Sugiyama, T., Irie, R., Wakamatsu, A., Hayashi, K., Sato, H., Nagai, K., Kimura, K., Makita, H., Sekine, M., Obayashi, M., Nishi, T., Shibahara, T., Tanaka, T., Ishii, S., Yamamoto, J., Saito, K., Kawai, Y., Isono, Y., Nakamura, Y., Nagahari, K., Murakami, K., Yasuda, T., Iwayanagi, T., Wagatsuma, M., Shiratori, A., Sudo, H., Hosoiri, T., Kaku, Y., Kodaira, H., Kondo, H., Sugawara, M., Takahashi, M., Kanda, K., Yokoi, T., Furuya, T., Kikkawa, E., Omura, Y., Abe, K., Kamihara, K., Katsuta, N., Sato, K., Tanikawa, M., Yamazaki, M., Ninomiya, K., Ishibashi, T., Yamashita, H., Murakawa, K., Fujimori, K., Tanai, H., Kimata, M., Watanabe, M., Hiraoka, S., Chiba, Y., Ishida, S., Ono, Y., Takiguchi, S., Watanabe, S., Yosida, M., Hotuta, T., Kusano, J., Kanehori, K., Takahashi-Fujii, A., Hara, H., Tanase, T., Nomura, Y., Togiya, S., Komai, F., Hara, R., Takeuchi, K., Arita, M., Imose, N., Musashino, K., Yuuki, H., Oshima, A., Sasaki, N., Aotsuka, S., Yoshikawa, Y., Matsunawa, H., Ichihara, T., Shiohata, N., Sano, S., Moriya, S., Momiyama, H., Satoh, N., Takami, S., Terashima, Y., Suzuki, O., Nakagawa, S., Senoh, A., Mizoguchi, H., Goto, Y., Shimizu, F., Wakebe, H., Hishigaki, H., Watanabe, T., Sugiyama, A., Takemoto, M., Kawakami, B., Yamazaki, M., Watanabe, K., Kumagai, A., Itakura, S., Fukuzumi, Y., Fujimori, Y., Komiyama, M., Tashiro, H., Tanigami, A., Fujiwara, T., Ono, T., Yamada, K., Fujii, Y., Ozaki, K., Hirao, M., Ohmori, Y., Kawabata, A., Hikiji, T., Kobatake, N., Inagaki, H., Ikema, Y., Okamoto, S., Okitani, R., Kawakami, T., Noguchi, S., Itoh, T., Shigeta, K., Senba, T., Matsumura, K., Nakajima, Y., Mizuno, T., Morinaga, M., Sasaki, M., Togashi, T., Oyama, M., Hata, H., Watanabe, M., Komatsu, T., Mizushima-Sugano, J., Satoh, T., Shirai, Y., Takahashi, Y., Nakagawa, K., Okumura, K., Nagase, T., Nomura, N., Kikuchi, H., Masuho, Y., Yamashita, R., Nakai, K., Yada, T., Nakamura, Y., Ohara, O., Isogai, T., and Sugano, S. (2004) Complete sequencing and characterization of 21,243 full-length human cDNAs. *Nat. Genet.* **36,** 40–45
16. Baehner, R. L., and Nathan, D. G. (1968) Quantitative nitro blue tetrazolium test in chronic granulomatous disease. *N. Engl. J. Med.* **278,** 971–976
17. Panchuk-Voloshina, N., Haugland, R. P., Bishop-Stewart, J., Bhalgat, M. K., Millard, P. J., Mao, F., Leung, W.-Y., and Haugland, R. P. (1999) Alexa dyes, a series of new fluorescent dyes that yield exceptionally bright, photostable conjugates. *J. Histochem. Cytochem.* **47,** 1179–1188
18. Choi, H. S., Kim, J. W., Cha, Y.-N., and Kim, C. (2006) A quantitative nitro blue tetrazolium assay for determining intracellular superoxide anion production in phagocytic cells. *J. Immunoassay Immunochem.* **27,** 31–44
19. Check, J., Byrd, C. L., Menio, J., Rippe, R. A., Hines, I. N., and Wheeler, M. D. (2010) Src kinase participates in LPS-induced activation of NADPH oxidase. *Mol. Immunol.* **47,** 756–762
20. Russell, D. G., Vanderven, B. C., Glennie, S., Mwandumba, H., and Heyderman, R. S. (2009) The macrophage marches on its phagosome: dynamic assays of phagosome function. *Nat. Rev. Immunol.* **9,** 594–600
21. Zhu, Q.-S., Xia, L., Mills, G. B., Lowell, C. A., Touw, I. P., and Corey, S. J. (2006) G-CSF induced reactive oxygen species involves Lyn-PI3-kinase-Akt and contributes to myeloid cell growth. *Blood* **107,** 1847–1856
22. Zhang, Y., Hoppe, A. D., and Swanson, J. A. (2010) Coordination of Fc receptor signaling regulates cellular commitment to phagocytosis. *Proc. Natl. Acad. Sci. U.S.A.* **107,** 19332–19337
23. Marshall, J. G., Booth, J. W., Stambolic, V., Mak, T., Balla, T., Schreiber, A. D., Meyer, T., and Grinstein, S. (2001) Restricted accumulation of phosphatidylinositol 3-kinase products in a plasmalemmal subdomain during Fc γ receptor-mediated phagocytosis. *J. Cell Biol.* **153,** 1369–1380
24. Bohdanowicz, M., Schlam, D., Hermansson, M., Rizzuti, D., Fairn, G. D., Ueyama, T., Somerharju, P., Du, G., and Grinstein, S. (2013) Phosphatidic acid is required for the constitutive ruffling and macropinocytosis of phagocytes. *Mol. Biol. Cell* **24,** 1700–1712
25. Suh, C.-I., Stull, N. D., Li, X. J., Tian, W., Price, M. O., Grinstein, S., Yaffe, M. B., Atkinson, S., and Dinauer, M. C. (2006) The phosphoinositide-binding protein p40phox activates the NADPH oxidase during FcγIIA receptor-induced phagocytosis. *J. Exp. Med.* **203,** 1915–1925
26. Vieira, O. V., Botelho, R. J., Rameh, L., Brachmann, S. M., Matsuo, T., Davidson, H. W., Schreiber, A., Backer, J. M., Cantley, L. C., and Grinstein, S. (2001) Distinct roles of class I and class III phosphatidylinositol 3-kinases in phagosome formation and maturation. *J. Cell Biol.* **155,** 19–25
27. Inanami, O., Johnson, J. L., McAdara, J. K., Benna, J. E., Faust, L. R., Newburger, P. E., and Babior, B. M. (1998) Activation of the leukocyte NADPH oxidase by phorbol ester requires the phosphorylation of p47PHOX on serine 303 or 304. *J. Biol. Chem.* **273,** 9539–9543
28. Oancea, E., and Meyer, T. (1998) Protein kinase C as a molecular machine for decoding calcium and diacylglycerol signals. *Cell* **95,** 307–318
29. Perisic, O., Wilson, M. I., Karathanassis, D., Bravo, J., Pacold, M. E., Ellson, C. D., Hawkins, P. T., Stephens, L., and Williams, R. L. (2004) The role of phosphoinositides and phosphorylation in regulation of NADPH oxidase. *Adv. Enzyme Regul.* **44,** 279–298
30. Nauseef, W. M. (2004) Assembly of the phagocyte NADPH oxidase. *Histochem. Cell Biol.* **122,** 277–291
31. Brown, G. E., Stewart, M. Q., Liu, H., Ha, V.-L., and Yaffe, M. B. (2003) A novel assay system implicates PtdIns(3,4)P_2, PtdIns(3)P, and PKCδ in intracellular production of reactive oxygen species by the NADPH oxidase. *Mol. Cell* **11,** 35–47
32. Morita, S. Y., Ueda, K., and Kitagawa, S. (2009) Enzymatic measurement of phosphatidic acid in cultured cells. *J. Lipid Res.* **50,** 1945–1952
33. Henry, R. M., Hoppe, A. D., Joshi, N., and Swanson, J. A. (2004) The uniformity of phagosome maturation in macrophages. *J. Cell Biol.* **164,** 185–194
34. Zha, Y., Marks, R., Ho, A. W., Peterson, A. C., Janardhan, S., Brown, I., Praveen, K., Stang, S., Stone, J. C., and Gajewski, T. F. (2006) T cell anergy is reversed by active Ras and is regulated by diacylglycerol kinase-α. *Nat. Immunol.* **7,** 1166–1173
35. Zhong, X. P., Guo, R., Zhou, H., Liu, C., and Wan, C. K. (2008) Diacylglycerol kinases in immune cell function and self-tolerance. *Immunol. Rev.* **224,** 249–264
36. Afzal, M., Matsugo, S., Sasai, M., Xu, B., Aoyama, K., and Takeuchi, T. (2003) Method to overcome photoreaction, a serious drawback to the use of dichlorofluorescin in evaluation of reactive oxygen species. *Biochem. Biophys. Res. Commun.* **304,** 619–624
37. DiGregorio, K. A., Cilento, E. V., and Lantz, R. C. (1987) Measurement of superoxide release from single pulmonary alveolar macrophages. *Am. J. Physiol.* **252,** C677–C683
38. Goebel, W. S., and Dinauer, M. C. (2002) Retroviral-mediated gene transfer and nonmyeloablative conditioning: studies in a murine X-linked chronic granulomatous disease model. *J. Pediatr. Hematol. Oncol.* **24,** 787–790
39. Wattenberg, B. W., and Raben, D. M. (2007) Diacylglycerol kinases put the brakes on immune function. *Sci. STKE 2007,* pe43
40. DiGregorio, K. A., Cilento, E. V., and Lantz, R. C. (1987) Measurement of superoxide release from single pulmonary alveolar macrophages. *Am. J. Physiol.* **252,** C677–C683
41. Li, X. J., Tian, W., Stull, N. D., Grinstein, S., Atkinson, S., and Dinauer, M. C. (2009) A fluorescently tagged C-terminal fragment of p47phox detects NADPH oxidase dynamics during phagocytosis. *Mol. Biol. Cell* **20,** 1520–1532
42. Ueyama, T., Kusakabe, T., Karasawa, S., Kawasaki, T., Shimizu, A., Son, J., Leto, T. L., Miyawaki, A., and Saito, N. (2008) Sequential binding of cytosolic Phox complex to phagosomes through regulated adaptor proteins: evaluation using the novel monomeric Kusabira-Green System and live imaging of phagocytosis. *J. Immunol.* **181,** 629–640
43. Yaffe, M. B. (2002) The p47phox PX domain: two heads are better than one! *Structure* **10,** 1288–1290

44. Ueyama, T., Lennartz, M. R., Noda, Y., Kobayashi, T., Shirai, Y., Rikitake, K., Yamasaki, T., Hayashi, S., Sakai, N., Seguchi, H., Sawada, M., Sumimoto, H., and Saito, N. (2004) Superoxide production at phagosomal cup/phagosome through βI protein kinase C during FcγR-mediated phagocytosis in microglia. *J. Immunol.* **173,** 4582–4589
45. Perry, D. K., Hand, W. L., Edmondson, D. E., and Lambeth, J. D. (1992) Role of phospholipase D-derived diradylglycerol in the activation of the human neutrophil respiratory burst oxidase. Inhibition by phosphatidic acid phosphohydrolase inhibitors. *J. Immunol.* **149,** 2749–2758
46. Scott, C. C., Dobson, W., Botelho, R. J., Coady-Osberg, N., Chavrier, P., Knecht, D. A., Heath, C., Stahl, P., and Grinstein, S. (2005) Phosphatidylinositol-4,5-bisphosphate hydrolysis directs actin remodeling during phagocytosis. *J. Cell Biol.* **169,** 139–149
47. Tyagi, S. R., Uhlinger, D. J., Lambeth, J. D., Champagne, C., and Van Dyke, T. E. (1992) Altered diacylglycerol level and metabolism in neutrophils from patients with localized juvenile periodontitis. *Infect. Immun.* **60,** 2481–2487
48. White, J. R., and Zembryki, D. (1989) Differentiation of second messenger systems in mast cell activation. *Agents Actions* **27,** 410–413
49. Zhong, X.-P., Hainey, E. A., Olenchock, B. A., Jordan, M. S., Maltzman, J. S., Nichols, K. E., Shen, H., and Koretzky, G. A. (2003) Enhanced T cell responses due to diacylglycerol kinase ζ deficiency. *Nat. Immunol.* **4,** 882–890